Effects of *E*×*B* drift on electron transport across the magnetic field in a miniature microwave discharge neutralizer

Kenta Hiramoto[1], Yuichi Nakagawa[2], Hiroyuki Koizumi[3], and Yoshinori Takao[4a]

[1]*Department of Systems Integration, Yokohama National University, Yokohama 240-8501, Japan*

[2]*Department of Aeronautics and Astronautics, The University of Tokyo, Bunkyo, Tokyo 113-8656, Japan*

[3]*Department of Advanced Energy, The University of Tokyo, Kashiwa, Chiba 277-8561, Japan*

[4]*Division of Systems Research, Yokohama National University, Yokohama 240-8501, Japan*

ABSTRACT

Using a three-dimensional particle-in-cell model, electron transport across a magnetic field has been investigated by obtaining the time-varying electric field and plasma parameters in a miniature microwave discharge neutralizer. The size of the neutralizer is 20 × 20 × 4 mm^3. Inside is a ring-shaped antenna producing 4.2 GHz microwaves, and permanent magnets for xenon plasma discharges. There are four orifices for electron extraction. The simulation area consists of both the discharge chamber and the vacuum region for the extraction. The numerical results show that radial striped patterns occur where the peak electron density is obtained, and the patterns seem to rotate in the azimuthal direction. This characteristic

[a] takao-yoshinori-yk@ynu.jp

structure is very similar to recent results obtained in Hall thrusters, and is probably due to the electron drift instability. Owing to the plasma structure, the azimuthal electric field is generated, which results in the $\boldsymbol{E}\times\boldsymbol{B}$ drift velocity in the axial direction with the radial magnetic field of the permanent magnets. This $\boldsymbol{E}\times\boldsymbol{B}$ drift velocity is a key factor in the electron transport across the magnetic field, leading to the electron extraction from the discharge chamber.

Electron sources are used for various devices such as x-ray tubes,[1] field emission displays,[2] etching tools,[3] nuclear fusion reactors,[4] and space propulsion.[5] For electrostatic propulsion devices like ion and Hall thrusters, electron sources are one of the indispensable components for neutralization of ion beams in order to obtain the thrust in space. The micro electron source reported here is a microwave discharge neutralizer for a miniature ion propulsion system (MIPS), which was mounted on 50 kg-class spacecraft, and successfully operated in space in 2014.[6,7] In contrast to conventional neutralizers which normally use hollow cathodes, the MIPS employs electron cyclotron resonance (ECR) discharges with ring-shaped permanent magnets and a 4.2 GHz microwave antenna, and thus can use even water as a propellant.[8]

Although the operation of the MIPS in space was demonstrated, the mechanism of electron transport across the magnetic field is still unclear. It needs to be elucidated in order to improve the neutralizer performance, which would result in better mass utilization efficiency and higher specific impulse for the ion propulsion system. Electron confinement by the magnetic field is important to effectively maintain the plasma discharge in a small chamber, while the confinement would also disturb electron extraction. Cross-field transport of electrons has been investigated for many years in various $\boldsymbol{E}\times\boldsymbol{B}$ devices, such as Hall thrusters,[9,10] magnetron discharges,[11] among others,[12-14] but the configuration of this MIPS is different from those devices.

Since it is almost impossible to observe how an electron moves across the magnetic field in experiments, particle simulations could be a powerful tool to investigate the electron transport. Although there are many papers on particle-in-cell simulations in two-dimensional configurations; e.g., *r*-*z* and *z*-θ two dimensional models for Hall thrusters[15,16] and dc magnetrons,[17] three-dimensional simulations are rarely conducted because of the extensive calculation time required. In this study, we took advantage of the small size of the discharge chamber as shown in Fig. 1, and developed a three-dimensional fully kinetic particle-in-cell (full-PIC) code. We use a real mass ratio of an electron to an ion, with which some simulations were conducted for xenon plasma discharges[18] and electron extraction of the neutralizer.[19,20] Our calculation model consists of both the plasma discharge region and the vacuum region, so that no assumptions are required for the electron extraction. Moreover, owing to the three-dimensional model, we could simultaneously obtain the fluctuations of the azimuthal electric field and the mirror magnetic confinement in the radial direction, which cannot be performed in the two-dimensional models.

In the previous work, we investigated the effects of the electrostatic fields, the microwave electromagnetic field, and the magnetostatic field of the permanent magnets, and found that electrons could not be extracted without the effect of the electrostatic field inside the plasma source.[19] Moreover, the $\boldsymbol{E}\times\boldsymbol{B}$ drift velocity near the orifice edge was found to be one of the important factors for electron extraction; this was found on analyzing the time-averaged distribution of the $\boldsymbol{E}\times\boldsymbol{B}$ drift velocity at the orifice plate and what region the

electrons mainly passed through inside the orifice.[20] However, the mechanism of the electron transport across the magnetic field, and the potential barrier from inside of the plasma source toward the orifice plate, remained elusive. In this study, we have investigated the time-varying electric field and plasma parameters, and found that the azimuthal electric fields and the radial magnetic field produces the $\boldsymbol{E}\times\boldsymbol{B}$ drift velocity in the axial direction, causing the cross-field transport and extraction of electrons.

The plasma source has a volume of 20 × 20 × 4 mm^3 with a ring-shaped antenna and permanent magnets. The orifice plate for electron extraction is located downstream of the plasma source. It has a thickness of 0.6 mm and four orifices, each with diameter 2.2 mm. The vacuum region is placed downstream of the orifice plate, and has a volume of 20 × 20 × 5.4 mm^3. This configuration is the same as that employed in our previous papers,[19,20] and is shown in Fig. 1 together with the magnetic field lines obtained by ANSYS Emag™ software; the magnetic field was obtained in cylindrical coordinates because of the axisymmetric structure of the ring-shaped permanent magnets.

In this study, we have conducted particle-in-cell simulations with Monte Carlo collisions (PIC/MCC) for kinetics of charged particles, and a finite-difference time-domain method (FDTD) for the electromagnetic fields of microwaves, under the following assumptions: (i) Only singly charged xenon ions Xe^+ and electrons are treated as particles; (ii) Neutral particles are spatially and temporally uniform with a Maxwellian velocity distribution at a gas temperature of 300 K; (iii) The reactions between charged particles and neutral ones

This manuscript was accepted by Phys. Plasmas. Click here to see the version of record.

are elastic, excitation, and ionization collisions for electrons,[21-23] and elastic and charge exchange collisions for ions;[24] (iv) The magnetic fields of microwaves are negligibly small compared with the magnetostatic fields of the magnets; (v) The potential on the entire wall boundary is zero, and the potential at z = 10 mm is set at 20 V for the electron extraction voltage, representing the electron-collector plate for the current measurement in our previous experiment.[25]

The above conditions are the same as those in our previous studies.[19,20] However, the grid spacing is set at 0.1 mm in this paper, which is half of the previous one, to allow for investigation of the fine structure of the plasma distributions. We employed the same numerical parameters and procedures as previously,[18] except for the grid spacing. Owing to the configuration of the microwave antenna and four orifices as shown in the inset of Fig. 1, we can assume a quarter symmetry with respect to the center of the antenna (the x-y origin), and treat only the first quadrant of the x-y plane as the simulation area to reduce the calculation time. Although we treat only this first quadrant, the number of simulation cells is more than four times larger than that employed in Ref. 18. Thus, the total computation time is more than a month, despite parallel computation on a workstation with four 3.0 GHz processors. It should be noted that the boron nitride (BN) dielectric is placed between the antenna and the orifice plate at the center of the discharge chamber. This BN is placed to suppress numerical noise at the z-axis. Since a ring-shaped profile of the plasma density is obtained, and the density at the center is very low (See Fig. 8 in Ref. 18), the existence of the

This manuscript was accepted by Phys. Plasmas. Click here to see the version of record.

BN has almost no effect on the plasma discharge. We have also confirmed that numerical results are identical with and without the BN.

To investigate the mechanism of electron transport across the magnetic field, we first obtained the steady-state solution of a xenon plasma discharge at a gas pressure of 1 mTorr, and for absorbed power of 0.3 W. Once the steady-state solution was obtained, we focused on the motion of a single electron, which was extracted from the plasma source to the outside through one of the orifices. Figure 2 shows a typical example of the time evolution of the guiding-center z position (thin line) and rA_θ for the single electron, where $r = \sqrt{x^2 + y^2}$ is the guiding-center position of the electron in cylindrical coordinates and A_θ is the azimuthal component of the vector potential obtained at the electron position. In cylindrical coordinates, contour lines of rA_θ correspond to the magnetic field lines as shown in Fig. 1; as long as the electron moves along the same magnetic field line, the value of rA_θ remains unchanged. In other words, if the electron moves across the magnetic field, the value of rA_θ changes. When the value of rA_θ is below about 2×10^{-7} Tm^2 near the orifice region, the electron goes outside of the plasma source to the vacuum region ($z > 4.6$ mm) in this study, and thus the electron is extracted at about 260 ns in Fig. 2. In this figure, the solid thick line indicates the PIC simulation results, while the dashed line is the theoretical trajectory determined by the $\boldsymbol{E}\times\boldsymbol{B}$ drift effect alone. The displacement of a function $f(\boldsymbol{x})$, is obtained from $\delta f = \nabla f \cdot \delta \boldsymbol{x} = \nabla f \cdot \boldsymbol{v}\delta t$ for position $\boldsymbol{x}$, velocity $\boldsymbol{v}$, and time t. Therefore, the value of rA_θ at time $t = t_1$ is given by

This manuscript was accepted by Phys. Plasmas. Click here to see the version of record.

$$rA_\theta(t_1) = \int_0^1 \delta(rA_\theta) + rA_\theta(t_0) = \int_{t_0}^{t_1} \nabla(rA_\theta) \cdot \boldsymbol{v}_{\boldsymbol{E}\times\boldsymbol{B}}(t)dt + rA_\theta(t_0), \quad (1)$$

where $\boldsymbol{v}_{\boldsymbol{E}\times\boldsymbol{B}}(t) = \boldsymbol{E}(\boldsymbol{r}(t)) \times \boldsymbol{B}(\boldsymbol{r}(t))/\{\boldsymbol{B}(\boldsymbol{r}(t))\}^2$ is the $\boldsymbol{E}\times\boldsymbol{B}$ drift velocity. Note that the theoretical $\boldsymbol{E}\times\boldsymbol{B}$ electron trajectory is obtained piecewise; after each collision, the velocity vector and the guiding center of the electron are changed, and the trajectory is obtained by setting the new guiding center r, as the initial condition of $rA_\theta(t_0)$ in Eq. (1). As shown in Fig. 2, both the solid thick line and the dashed line follow almost identical trajectories. Moreover, there was almost no difference in the trajectory although we calculated the effect of the polarization drift. Hence, the time evolution of rA_θ, or the electron transport across the magnetic field, is mainly caused by the $\boldsymbol{E}\times\boldsymbol{B}$ drift effect, rather than by collisions.

Shown in Fig. 3(a) are the distributions of the electron density n_e, and the electric-field vectors at z = 2.0 mm, where the results are averaged over 100 microwave cycles. The solid line indicates the orifice edge, and the dashed lines represent the boundaries of the permanent magnets (See Fig. 1). Compared to the results determined by averaging over 50,000 microwave cycles in our previous paper,[18] the characteristic structure of striped patterns can be seen here between r = 4 and 6 mm. Here, the peak electron density is obtained downstream of the ring-shaped antenna, and this striped structure is similar to the plasma distribution in a magnetic filter (e.g., Fig. 10 in Ref. 26) and in Hall thrusters.[10] As shown in Figs. 3(a)–(d), we have observed the time variation of these distributions. We found that the structure rotates in a clockwise direction at the x-y plane, which is the same direction of the

grad-B and curvature drift for electrons. An azimuthal rotation of plasma density has been reported for various $\boldsymbol{E}\times\boldsymbol{B}$ devices,[9-14] although those configurations are different from ours. It is notable that these striped patterns can be observed when the results are averaged over only one microwave cycle, although the distributions contain larger numerical fluctuations due to the fewer particles per cell. Similar striped patterns are also observed for the ion density, the electron temperature T_e, and the potential ϕ. Owing to the potential distributions, the azimuthal electric fields exist at around r = 4 – 6 mm as shown in Fig. 3(a). Since the magnetic fields are directed in the positive r direction at around r = 5 mm (See Fig. 1), the azimuthal electric fields in the clockwise direction induce the $\boldsymbol{E}\times\boldsymbol{B}$ drift velocity in the positive z direction.

Figure 3(e) shows the electric-field vectors averaged over 50,000 microwave cycles at z = 2.0 mm, where the lengths of all vectors are set to be equal to show the direction clearly. Despite the quarter symmetry with respect to the center of the antenna, the point of symmetry for the electric field does not exit at the center of the orifice; rather, it exits on the counterclockwise side of the orifice (x = 2.7 mm and y = 3.3 mm), which indicates that the electric field in the clockwise direction somewhat dominates over that in the counterclockwise direction. This tendency was also confirmed at the x-y plane for z = 2.5, 3.0, and 3.5 mm with the point of symmetry moving to the positive r direction. These distributions of the electric and magnetic fields would contribute to the electron transport across the magnetic field toward the inlet of the orifices.

Since the striped patterns shown in Figs. 3(a)–(d) are very similar to recent results obtained with Hall thrusters, we have analyzed the mechanisms for what causes these patterns using the dispersion relation based on kinetic theory.[27-29] As shown in Figs. 3(a)–(d), the wavelength and frequency of the stripes are estimated to be about 0.55 mm and 4.7 MHz, respectively; the resultant phase velocity is calculated to be 2.6×10^3 m/s. From Eqs. (7), (8), and (10) in Ref. 27, the most unstable wavenumber, wave frequency, and phase velocity are $k_{max} = 1/\sqrt{2}\lambda_{De}$, $\omega_R = \omega_{pi}/\sqrt{3}$, and $v_{phase} = \sqrt{2/3}c_s$, respectively. Here, λ_{De} is the electron Debye length, ω_{pi} is the ion plasma frequency, and c_s is the ion sound speed, $\sqrt{qT_e/M}$ with the elementary charge q, and the ion mass M. In the region showing the stripes obtained from our PIC simulations, the electron density and temperature are about 1.8×10^{17} m^{-3} and 13 eV, respectively, which results in a wavelength of 0.56 mm, a wave frequency of 4.5 MHz, and a phase velocity of 2.5×10^3 m/s based on the dispersion relation. These values are in good agreement with the above estimations, and thus the theory in Refs. [27-29] could be applicable to the results from the MIPS plasma source. This implies that the electron drift instability seen in Hall thrusters is also related to these striped patterns we see in the MIPS.

However, the configuration of the MIPS is different from that of Hall thrusters. There is no applied dc voltage in the axial direction of the MIPS, and its magnetic field is about one order of magnitude higher than that of typical Hall thrusters. This configuration produces lower azimuthal $\boldsymbol{E}\times\boldsymbol{B}$ drift velocities than in Hall thrusters; its values are calculated to be lower than about 6.0×10^2 m/s for the axial electric field and the radial magnetic field

obtained in our PIC simulations. While the azimuthal $\boldsymbol{E}\times\boldsymbol{B}$ drift velocity is slow, the total azimuthal electron drift velocity in our PIC simulation exceeds 1.0×10^5 m/s. This high electron drift velocity results in a large flow difference between the ions and electrons, and probably provides the driving force for the instability (like Hall thrusters), although the mechanism of the high electron drift velocity here is not the same as in Hall thrusters. Investigation of this mechanism is left for future work.

We have also investigated the time-varying distributions of the potential and electron density on the θ-z plane at r = 5.0 mm (i.e., the pitch circle of the four orifices). Several results are show in Fig. 4, where the striped patterns of the potential are also seen at the θ-z plane in the plasma source. It should be noted that Fig. 4(b) shows the distribution of the electron density on a logarithmic scale to show the distribution outside of the plasma source. If the distribution is shown on a linear scale, we can confirm the existence of similar striped patterns for the electron density. However, these patterns are not the same for the entire time. They are time dependent; the high potential appears about every 5,000 microwave cycles (1.19 μs, about 1 MHz), and at this time the electrons are more easily extracted. This period is on the same order as the ion plasma frequency at a plasma density of 10^{16}–10^{17} m^{-3}, implying that the extraction mechanism of electrons is related to the ion-time-scale instability. In a non-uniform electric field, the $\boldsymbol{E}\times\boldsymbol{B}$ drift velocity also depends on the Larmor radius r_L, as the second term due to the finite-Larmor-radius effect, leading to a drift instability because of the

different ion and electron drift velocities.[30] The $\boldsymbol{E}\times\boldsymbol{B}$ drift velocity would induce not only the electron transport across the magnetic field, but also the time-varying extraction of electrons.

In conclusion, it is found that the $\boldsymbol{E}\times\boldsymbol{B}$ drift velocity plays an important role for the cross-field transport and extraction of electrons for a miniature microwave discharge neutralizer using a three-dimensional PIC/MCC method. In the plasma source, we have observed the characteristic striped patterns rotating in the azimuthal direction, which is probably due to the electron drift instability often seen in Hall thrusters. The striped patterns induce the potential difference in the azimuthal direction, which in turn causes the azimuthal electric fields, resulting in the $\boldsymbol{E}\times\boldsymbol{B}$ drift velocity in the positive z direction with the radial magnetostatic fields of permanent magnets. The $\boldsymbol{E}\times\boldsymbol{B}$ drift in this non-uniform electric field also leads to the drift instability, and thus the amount of electron extraction is found to depend on time. Since the $\boldsymbol{E}\times\boldsymbol{B}$ drift effect dominates over the collision effect, it might be possible to improve the neutralizer performance in terms of higher currents of extracted electrons if the magnetic field configurations were optimized. The increase in pressure (i.e., collision) would also result in higher electron currents. However, the neutralizer performance may be adversely affected in terms of the mass utilization efficiency and specific impulse of ion propulsion systems. Future studies should include investigation of the generation mechanisms of the high electron drift velocity, and optimization of the plasma source configuration for better electron extraction.

This work was financially supported in part by JSPS KAKENHI Grant Numbers JP25289304 and JP16H06370. Part of the computer simulations was performed on the KDK computer system at the Research Institute for Sustainable Humanosphere, Kyoto University.

[1] H. Sugie, M. Tanemura, V. Filip, K. Iwata, K. Takahashi, and F. Okuyama, Appl. Phys. Lett. **78,** 2578 (2001).

[2] M. Nagao and T. Yoshida, Microelectron. Eng. **132,** 14 (2015).

[3] P. L. G. Ventzek, M. Grapperhaus, and M. J. Kushner, J. Vac. Sci. Technol. B **12,** 3118 (1994).

[4] T. Imai, N. Kobayashi, R. Temkin, M. Thumm, M. Q. Tran, and V. Alikaev, Fusion Eng. Des. **55,** 281 (2001).

[5] D. M. Goebel and I. Katz, *Fundamentals of Electric Propulsion: Ion and Hall Thrusters* (Wiley, Hoboken, NJ, 2008).

[6] H. Koizumi, K. Komurasaki, J. Aoyama, and K. Yamaguchi, Trans. Jpn. Soc. Aeronaut. Space Sci., Aerosp. Technol. Jpn. **12,** Tb_19 (2014).

[7] H. Koizumi, H. Kawahara, K. Yaginuma, J. Asakawa, Y. Nakagawa, Y. Nakamura, S. Kojima, T. Matsuguma, R. Funase, J. Nakatsuka, and K. Komurasaki, Trans. Jpn. Soc. Aeronaut. Space Sci., Aerosp. Technol. Jpn. **14,** Pb_13 (2016).

[8] Y. Nakagawa, H. Kawahara, H. Koizumi, and K. Komurasaki, "Fundamental Experiments with Liquid Propellants for the Microwave-discharge Ion Thruster," in *Space Propulsion 2016* (Rome, Italy, 2016), SP2016_3125240.

[9] C. L. Ellison, Y. Raitses, and N. J. Fisch, Phys. Plasmas **19,** 013503 (2012).

[10] T. Lafleur, S. D. Baalrud, and P. Chabert, Phys. Plasmas **23,** 053502 (2016).

[11] A. Hecimovic, J. Phys. D **49,** 18LT01 (2016).

[12] T. Pierre, Phys. Plasmas **23,** 042110 (2016).

[13] O. D. Cortázar, A. Megía-Macías, O. Tarvainen, and H. Koivisto, Phys. Plasmas **22,** 123511 (2015).

[14] J.-P. Boeuf and B. Chaudhury, Phys. Rev. Lett. **111,** 155005 (2013).

[15] S. Cho, H. Watanabe, K. Kubota, S. Iihara, K. Fuchigami, K. Uematsu, and I. Funaki, Phys. Plasmas **22,** 103523 (2015).

[16] J. C. Adam, A. Héron, and G. Laval, Phys. Plasmas **11,** 295 (2003).

[17] E. Bultinck, I. Kolev, A. Bogaerts, and D. Depla, J. Appl. Phys. **103**, 013309 (2008).

[18] Y. Takao, H. Koizumi, K. Komurasaki, K. Eriguchi, and K. Ono, Plasma Sources Sci. Technol. **23,** 064004 (2014).

[19] Y. Takao, H. Koizumi, Y. Kasagi, and K. Komurasaki, Trans. Jpn. Soc. Aeronaut. Space Sci., Aerosp. Technol. Jpn. **14,** Pb_41 (2016).

[20] Y. Takao, K. Hiramoto, Y. Nakagawa, Y. Kasagi, H. Koizumi, and K. Komurasaki, Jpn. J. Appl. Phys. **55,** 07LD09 (2016).

[21] M. Hayashi, J. Phys. D **16,** 581 (1983).

[22] F. J. d. Heer, R. H. J. Jansen, and W. v. d. Kaay, J. Phys. B **12,** 979 (1979).

[23] D. Rapp and P. Englander-Golden, J. Chem. Phys. **43,** 1464 (1965).

[24] I. D. Boyd, J. Appl. Phys. **95,** 4575 (2004).

[25] Y. Takao, H. Koizumi, Y. Kasagi, and K. Komurasaki, "Investigation of Electron Extraction from a Microwave Discharge Neutralizer for a Miniature Ion Propulsion System," in *Joint Conference of 30th International Symposium on Space Technology and Science, 34th International Electric Propulsion Conference and 6th Nano-satellite Symposium* (Kobe-Hyogo, Japan, 2015),

IEPC-2015-159/ISTS-2015-b-159.

[26] J. P. Boeuf, B. Chaudhury, and L. Garrigues, Phys. Plasmas **19,** 113509 (2012).

[27] T. Lafleur, S. D. Baalrud, and P. Chabert, Plasma Sources Sci. Technol. **26,** 024008 (2017).

[28] T. Lafleur, S. D. Baalrud, and P. Chabert, Phys. Plasmas **23,** 053503 (2016).

[29] A. Ducrocq, J. C. Adam, A. Héron, and G. Laval, Phys. Plasmas **13,** 102111 (2006).

[30] F. F. Chen, *Introduction to Plasma Physics* (Plenum Press, New York, 1974), p. 32.

List of Figure Captions

FIG. 1. (Color online) Configuration of the neutralizer and distribution of the magnetic field lines (in black) at the z-r plane passing through the center of the orifice, together with the resonant magnetic field (thick line) of 0.15 T for 4.2 GHz microwaves. The inset shows the ring-shaped microwave antenna and the positions of the four orifices.

FIG. 2. (Color online) Transition of rA_θ for an electron; the solid thick line represents the PIC simulation result, the dashed line is determined by the analytical calculation based only on the $\boldsymbol{E}\times\boldsymbol{B}$ drift effect, and the thin line shows the guiding-center z position of the electron. Here, the vertical lines indicate the time when electron-neutral collisions occur. Since collisions change the velocity vector of the electron and the guiding-center position, the $\boldsymbol{E}\times\boldsymbol{B}$ electron trajectory is obtained piecewise. After each collision, the trajectory is calculated using Eq. (1) by setting the new guiding center r as the initial condition.

FIG. 3. (Color online) (a) Distributions of the electron density and electric-field vectors for the x-y plane at z = 2.0 mm. The solid line and the dashed lines represent the orifice edge and the boundaries of the permanent magnets, respectively. Time evolution of the striped patterns is displayed in (a)–(d) for the microwave cycles from 70100 to 71000, where open and closed

stars are added as visual guides. (e) Arrows of the electric fields averaged over 50,000 microwave cycles (11.9 μs), where the length of all the arrows are equal.

FIG. 4. (Color online) Time-varying distributions of (a) the potential, and (b) the electron density for the θ-z plane at r = 5.0 mm. The x axis is set at 0 degrees while the y axis is at 90 degrees, the orifice plate is displayed as the gray rectangles, and the electron density is plotted on a logarithmic scale.

This manuscript was accepted by Phys. Plasmas. Click here to see the version of record.

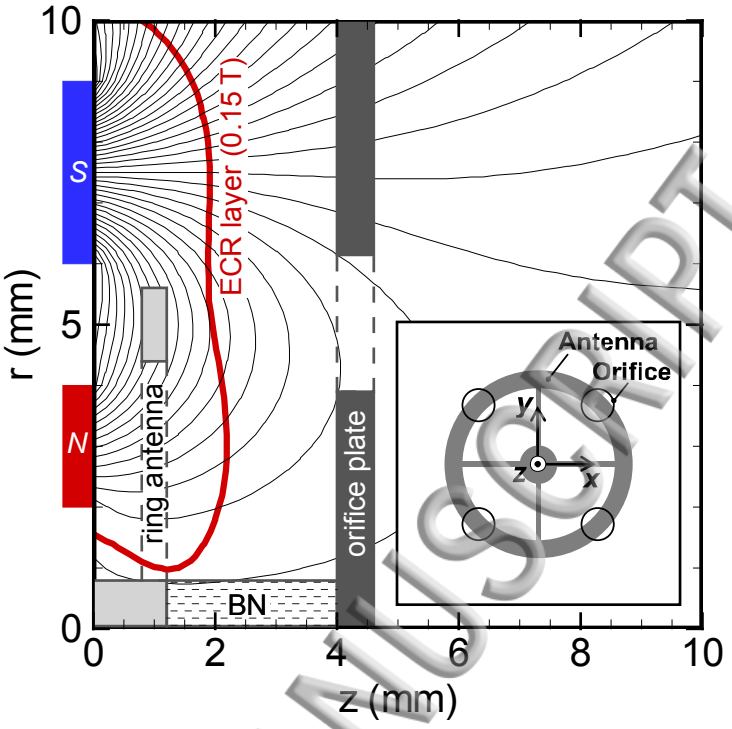

FIG. 1

(7.5 cm × 7.5 cm)

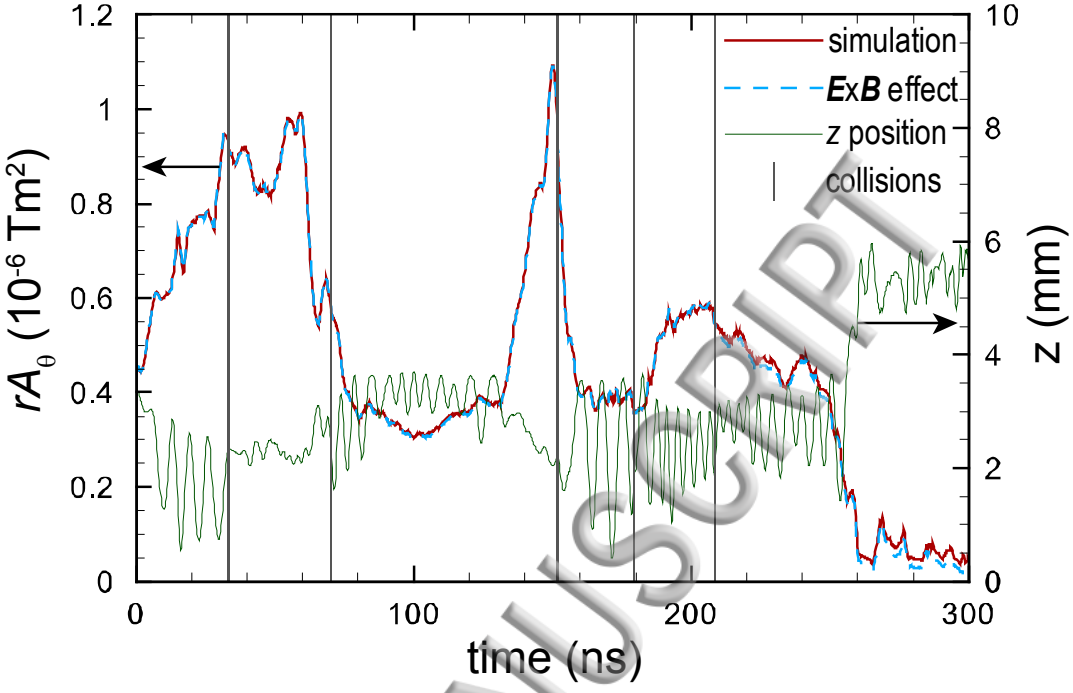

FIG. 2

(7.62 cm × 5 cm)

This manuscript was accepted by Phys. Plasmas. Click here to see the version of record.

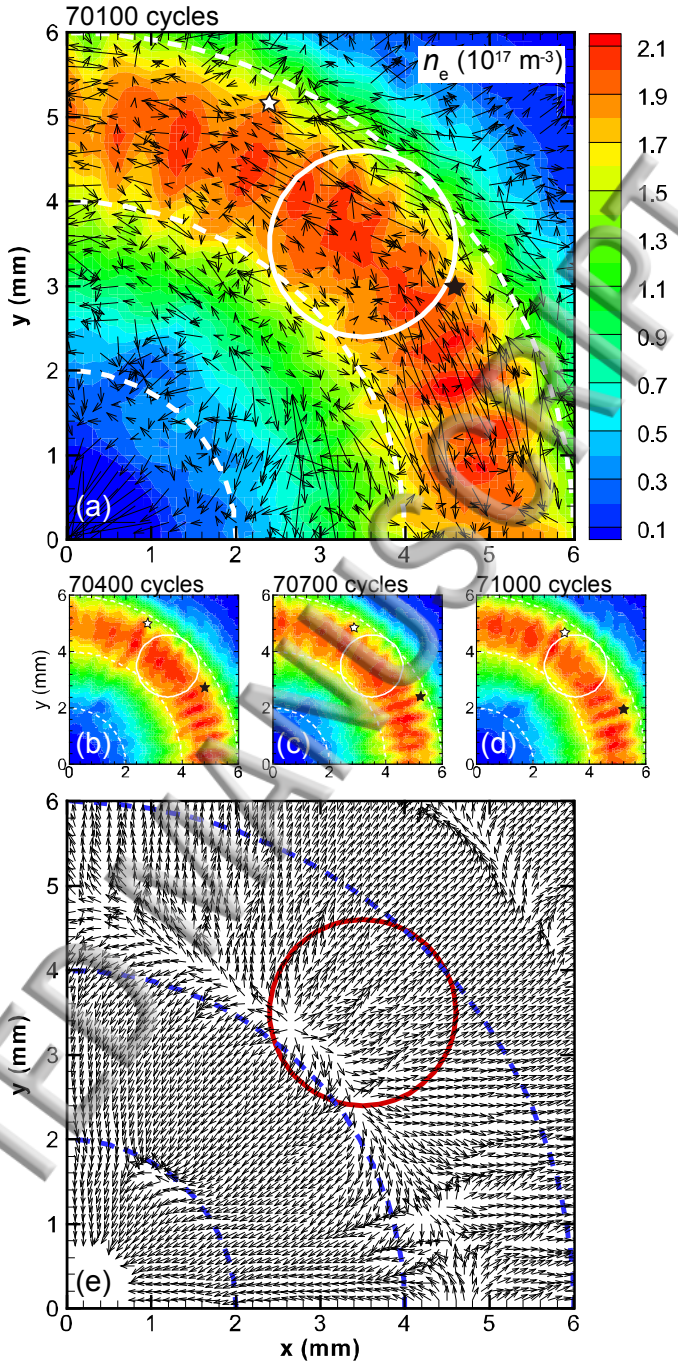

FIG. 3

(7.5 cm × 14.9 cm)

This manuscript was accepted by Phys. Plasmas. Click here to see the version of record.

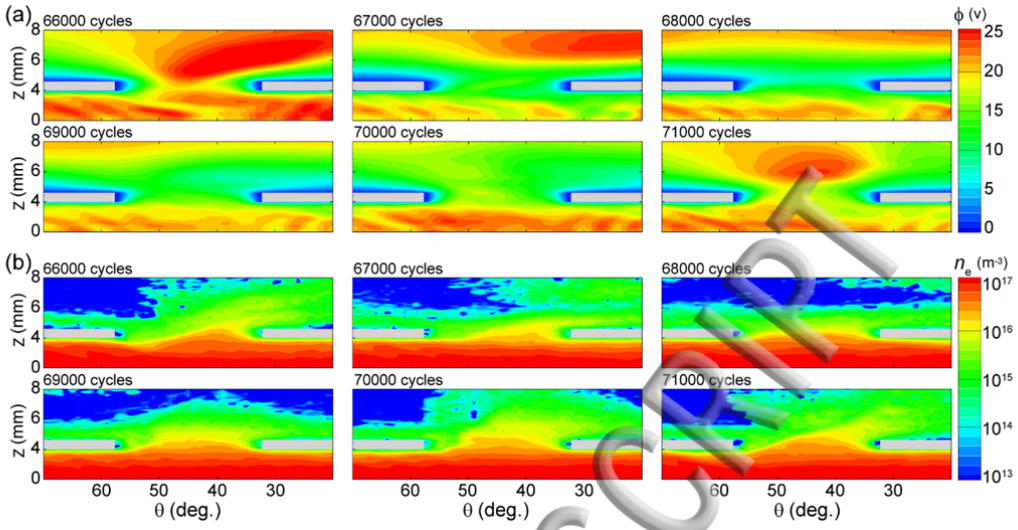

FIG. 4

(16.3 cm × 8.42 cm)

This manuscript was accepted by Phys. Plasmas. Click here to see the version of record.

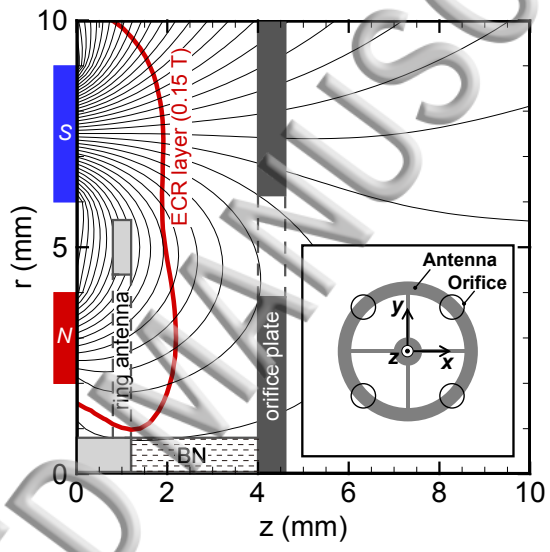

This manuscript was accepted by Phys. Plasmas. Click here to see the version of record.

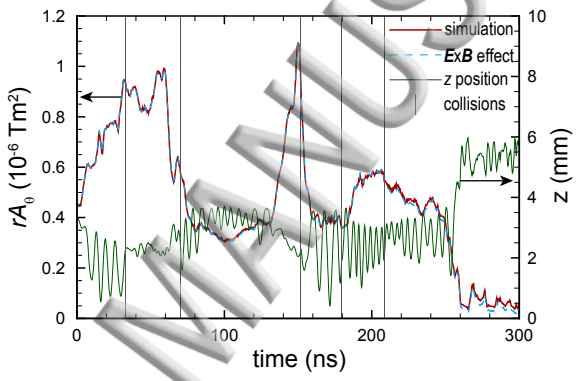

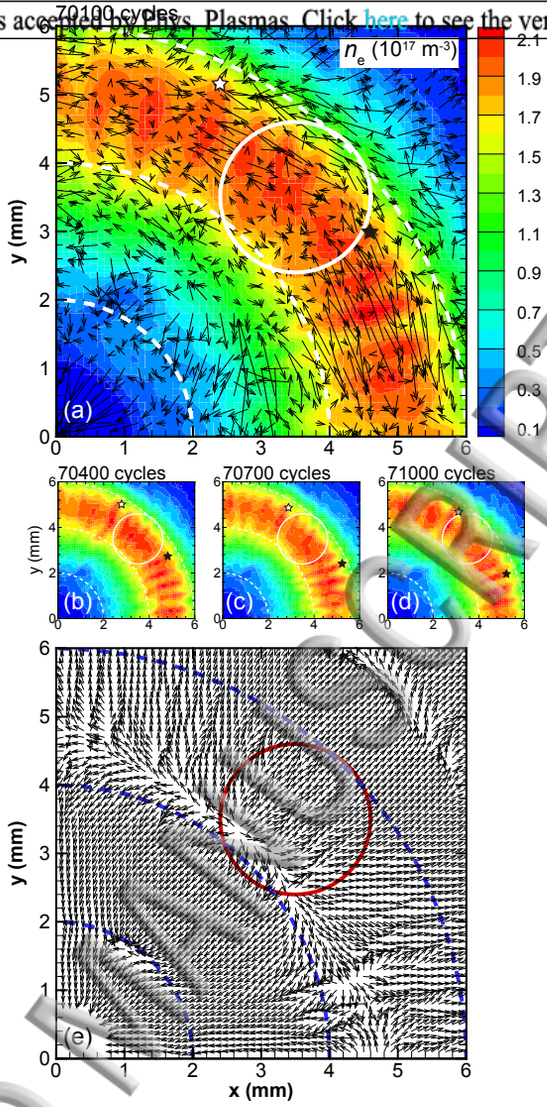

This manuscript was accepted by Phys. Plasmas. Click here to see the version of record.